A Micro-Acoustic Enhanced Low-Impedance Antenna System for IoT Wake-Up Receivers

Giuseppe Michetti, *Graduate Student Member, IEEE*, Luca Colombo, *Member, IEEE*, Gabriel Giribaldi, *Student Member, IEEE*, Ankit Mittal, *Graduate Student Member, IEEE*, Hussain Elkotby, *Member, IEEE*, Ravikumar Pragada, *Member, IEEE*, Aatmesh Shrivastava, *Senior Member, IEEE*, and Matteo Rinaldi, *Senior Member, IEEE*

***Abstract*—In this work, we propose a passive radio frequency (RF) front-end tailored for wake-up receivers (WuRx) to be deployed in cellular Internet of Things (IoT) devices and wearables networks, featuring a low radiation resistance antenna and a high-Q matching network implemented with microacoustic resonators integrated to obtain a systematic higher node's sensitivity at no cost in terms of power consumption. We show how these components can be co-designed to obtain high passive voltage gain, hardware-level blocker immunity, and increased resilience to integration parasitics, relaxing link budget for low-power IoT nodes. We report experimental validation of a PCB antenna with 2-dBi gain measured on an 11-Ω input resistance at resonance, and an in-house fabricated micro-electro-mechanical system (MEMS) thin-film aluminum nitride bulk acoustic resonator with a quality factor $Q = 550$ and a piezoelectric coupling coefficient $k_t^2 = 7\,\%$, hybridly integrated with a commercial off-the-shelf low-power WuRx circuit to benchmark the proposed RF front-end design at 850 MHz. We demonstrate a passive voltage gain of 12 dB due to the MEMS resonator, and an additional 11 dB due to the proposed antenna design (for a total of an unprecedented 2-dB passive gain in this frequency range) leading to an over the air −61-dBm minimum detectable input power and 23-dB blocker rejection.**

***Index Terms*—Internet of Things (IoT), micro-electro-mechanical system (MEMS) resonators, radio frequency (RF) antennas, RF envelope detectors, RF low-power receivers, RF matching network, wake up receivers.**

I. Introduction

THE FAST paced and worldwide evolution of wireless sensor networks [1], commonly referred to as Internet of Things (IoT) [2], has fostered research and development of novel radio frequency (RF) transceivers capable of mitigating power consumption and maintenance of IoT nodes, as well as extending sensitivity and communication range. As the latest trends confirm, billions of IoT devices [3] will be deployed all over the planet, tasked to collect data, often in remote areas where little if any human intervention is possible.

For these applications, novel radio paradigms are being investigated to reduce the power consumption of IoT nodes, typically limited by recovery and decoding of RF signals, so as to lower maintenance costs and ease deployment of a large number of devices. In this framework, wake-up receivers (WuRx) can be used to recover wake-up signals, that can ultimately be used to query asynchronous information from an IoT device with nW power consumption [4], [5], [6], [7]. WuRx s operate under completely different conditions and constraints than conventional receiver (Rx) circuitry, therefore, novel designs are needed to deploy RF front-ends that are specific to WuRx.

Typical power consumption for cellular IoT devices in IDLE mode, where they spend majority of their time waiting for a paging message, is in order of 10s of mW [8]. These devices have to tradeoff increased paging latency for reducing power consumption. On-demand, infrequent wake-up event features are not only critical for enhancing the battery life for IoT devices, but they also play an instrumental role in reducing paging latency [9], [10]. The vision to deploy WuRx on a large-scale and marketable platform has consolidated over the last two years with the emergence of IEEE802.11ba [11] that defines and regulates the operation of ultralow power architectures as part of the IEEE standard 802.11 (i.e., Wi-Fi®). Consequently, an increasing number of works are being published to provide early stage performance evaluation on event-driven networks [12], [13], [14] such as the ones discussed in this work.

In the growing narrow-band (NB) IoT spectrum, the frequency bands between 800 and 900 MHz (NB-IoT Bands 18, 19, and 20) are of great interest, as up and downlink segments are being allocated in the 3GPP release 13 [8], [15] to enhance cellular communication services supporting such low-power architectures. Even if the proposed technique is frequency agnostic, this work showcases devices and radio performance for an RF front-end operating around 820 MHz, demonstrating a systematic approach to obtain better performance in relevant low-power NB-IoT bands.

Micro-acoustic micro-electro-mechanical system (MEMS) resonators [16], [17], [18] have led the RF filter market for mobile radios throughout the 4G communication era, due to achievable mechanical quality factors in the order of 1000 s

Manuscript received 25 October 2022; revised 30 November 2022; accepted 16 December 2022. Date of publication 2 January 2023; date of current version 9 May 2023. This work was supported by the InterDigital Communications, Inc., Conshohocken, PA, USA. *(Corresponding author: Giuseppe Michetti.)*

Giuseppe Michetti, Luca Colombo, Gabriel Giribaldi, Ankit Mittal, Aatmesh Shrivastava, and Matteo Rinaldi are with the SMART Center, Northeastern University, Boston, MA 02115 USA (e-mail: michetti.g@northeastern.edu).

Hussain Elkotby and Ravikumar Pragada are with the Department of Future Wireless, InterDigital Communications, Inc., Conshohocken, PA 19428 USA.

Digital Object Identifier 10.1109/JIOT.2022.3233355

in the VHF range [19], in a compact form factor (typically few hundreds of μm^2 area) and with processes compatible with CMOS manufacturing, therefore, marketable when mass produced.

When implementing such resonators as matching elements at the WuRx interface, gains of 38 and 32 dB have been recently demonstrated using MEMS resonators, respectively, at 110 and 570 MHz by Colombo et al. [20].

In this article, propose a different take on the WuRx front end, highlighting the critical factors required to obtain large passive voltage amplification by co-designing matching networks and RF antennas to systematically improve WuRx performance. Through this work, we show substantial improvement of the front-end voltage amplification by lifting the limiting factors of each component via component co-design.

In Section II, we briefly cover the underlying assumptions of WuRx applications from a system perspective and how a novel approach to the RF front-end based on micro-acoustic resonators and co-designed antennas can be exploited for high voltage gain.

In Section III, we discussed to devise the proposed RF passives for the IoT node input stage on a PCB. The challenges posed by a non-50 Ω antenna measurements are discussed, as well as circuit-level integration constraints posed by PCB integration of MEMS resonators via wire bonds. In Section IV, we report the measurement results to validate the concepts previously covered, including an 11-Ω antenna design operating at 850 MHz and a thin-film bulk acoustic resonator (FBAR) fabricated on a 3-μm sputtered AlN film. Following, a simple WuRx circuit is built by integrating said components with commercial off-the-shelf circuits on a PCB, showcasing an 11-dB RF sensitivity improvement thanks to the proposed techniques, and enhanced spectral selectivity with 23-dB blocker rejection immunity measured against digital communication metrics.

Finally, Section V concludes this article with a summary of the techniques and results shown in this article.

II. Background

An extensive literature exists on ICs tailored for sub μW RF signal detection [5], [22], [23] and on high-Q MEMS resonators [20], [24], [25], [26] deployed to provide large passive voltage amplification. In this section, we analyze the RF input stage to highlight the scope of passive voltage optimization. Differently from previous works, we include the antenna resistance as a variable in the system, leading to a more generalized set of parameters required to maximize voltage gain at the WuRx input.

A rudimentary electrical model of a WuRx passive front-end is visualized in Fig. 1(a). This model is fundamentally different from conventional Rx equivalent circuits: conventional input stages, such as low noise amplifiers (LNAs), are designed with power-hungry transistor stages that typically exhibit a real impedance, that needs to be power-matched to the antenna impedance for maximum power transfer [27, Ch. 5]. The techniques discussed as follow strictly apply to IoT WuRx receivers that typically exhibit high capacitive impedance, and are not meant to be generalized to conventional RF receivers.

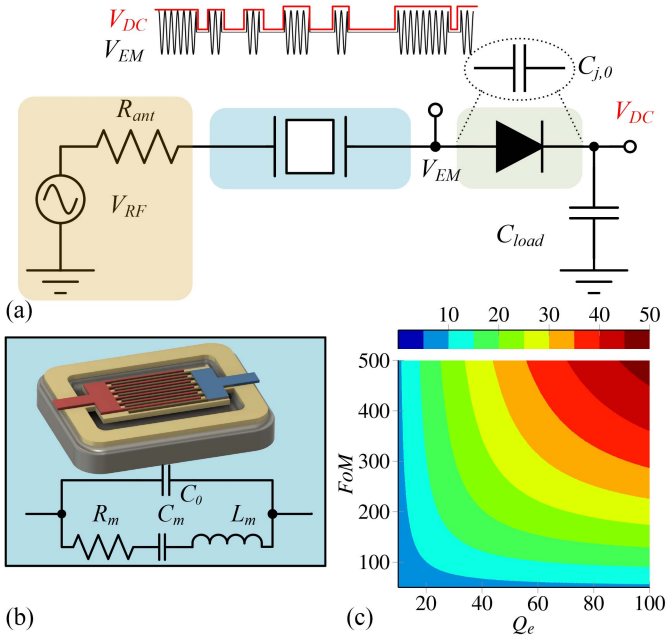

Fig. 1. WuRx RF front-end circuit-level schematic. (a) V_{RF} voltage is picked up by an antenna (yellow shaded), and it excites the nonlinearity of a rectifier when the V_{EM} amplitude exceeds a certain threshold V_{th}. When the information is coded into an amplitude-modulated signal, the envelope of the signal is reproduced as voltage on a load capacitor C_{load}, and it is, therefore, ready to be digitized. (b) Thin-film piezoelectric RF resonator deployed to resonate $C_{j,0}$. The BVD [21] electrical resonator model highlights the motional inductance L_m used to bring the circuit into resonance. (c) SPICE-level simulated voltage gain G_v, mapped in the color bar, for typical MEMS resonator FoM and external quality factors Q_e (discussed in Section II), MEMS capacitance $C_0 = C_{j,0}$, and electro-mechanical coupling coefficient $k_t^2 = 10\,\%$.

For low-power RF signals, the rectifier network is represented as the unbiased junction capacitance $C_{j,0}$ of a diode, as shown in Fig. 1, which is the most simple representation of a passive RF rectifier [28]. Above a voltage threshold V_{th}, the envelope of the RF output voltage V_{EM} in Fig. 1(a) is demodulated at the circuit output (V_{DC}), where it is held by C_{load} and it is, therefore, available for further low-power signal processing. The threshold V_{th} is limited by the chosen rectifier architecture and technology. Note that despite a diode rectifier being shown in the schematic in Fig. 1, various alternatives have been proposed [29] which are all functionally equivalent to the linearized $C_{j,0}$ model. The nonlinear dynamics of this network depend on the rectifier technology in use and a detailed circuit analysis is reported in [30] for diode rectifiers.

The linearized capacitor model does not take into account the rectifiers nonlinearity, therefore, it cannot predict demodulation efficiency and it is, therefore, valid for the input RF voltage $V_{\mathrm{RF}} \ll V_{\mathrm{th}}$. Despite its simplicity, this linearized model conveys enough information to determine the resonant small signal voltage gain, which is the focus of this work.

A strategy to boost V_{EM} in a WuRx with passive components is based on resonance: for this class of Rx circuits, components, such as inductors or MEMS resonators [Fig. 1(b)] are referred to as matching networks, even though there is

no power matching involved and they are effectively used to resonate out a capacitive impedance rather than transforming it in a classical sense. When using a one-port matching component, the voltage gain at resonance at the IC input G_v can be written as follows:

$$G_v = \left|\frac{V_{\text{EM}}}{V_{\text{RF}}}\right| \approx \frac{X_c}{R_{\text{ant}} + R_{\text{match}} + R_{\text{diss}}} \tag{1}$$

where X_c is the reactance associated to $C_{j,0}$, R_{match} the ohmic loss due to the matching network, and R_{diss} the ohmic loss due to the antenna. Equation (1) holds as long as $C_{\text{load}} \gg C_{j,0}$.

When an MEMS resonator is used as a series matching network [25] [Fig. 1(c)], the MEMS equivalent inductance is used to resonate $C_{j,0}$.

Starting from the equivalent electrical model for the MEMS resonator, known as Butterworth–Van–Dyke (BVD) model [in the inset of Fig. 1(b)], it is possible to derive G_v as a function Figure of Merit (FoM), $\text{FoM} = k_t^2 Q_m$ [31] of the MEMS resonator, where k_t^2 is the resonator coupling coefficient (representing the electro-acoustic energy transduction) and Q_m is the mechanical quality factor (representing the ratio between energy loss and energy stored per cycle at resonance).

For this network, an external quality factor Q_e can be written as follows:

$$Q_e = \frac{X_c}{R_{\text{ant}}}. \tag{2}$$

So that, for a sufficiently high Q_m, G_v can be simplified as follows:

$$G_v \approx \frac{Q_e}{1 + k_p \dfrac{Q_e}{\text{FoM}} + \dfrac{1 - \eta_{\text{ant}}}{\eta_{\text{ant}}}} \tag{3}$$

where η_{ant} represents the antenna efficiency, and k_p is a dimensionless parameter, function of $C_{j,0}$, k_t^2 and the MEMS resonator actuation capacitance C_0. k_p is a dimensionless factor ranging between 1 and 4, and it can be minimized by proper MEMS resonator sizing. In general, it is not possible to express k_p in closed form, so a more thorough discussion on k_p is found in [32].

Projected gain G_v achieved with MEMS technology is obtained via SPICE simulations in Fig. 1(c), confirming the trends analytically derived in Fig. 1.

From this discussion, $G_v \approx Q_e$ as long as $\text{FoM}/k_p \gg Q_e$.

III. Methods

Fig. 1 reveals that to provide large passive voltage not only a high FoM is required from the matching component, but also a large Q_e is required for the overall system, which can be obtained either by resonating a large load reactance X_c and/or by reducing antenna impedance R_{ant}. In this section, we discuss methodologies to tackle the implementation of RF input stages with high Q_e, targeting both axes of the design spaces. Therefore, we explore the co-design of: 1) low R_{ant} antennas (LRA) and 2) MEMS matching networks suitable to resonate out large X_c, with a focus on the impact of their integration with RF PCBs.

In the following, we show that simple modifications of well-known antenna designs can be used to achieve the required antenna impedance. The discussion is limited to conventional substrates and planar designs, to comply with the low cost and mass-scalable technologies required in IoT.

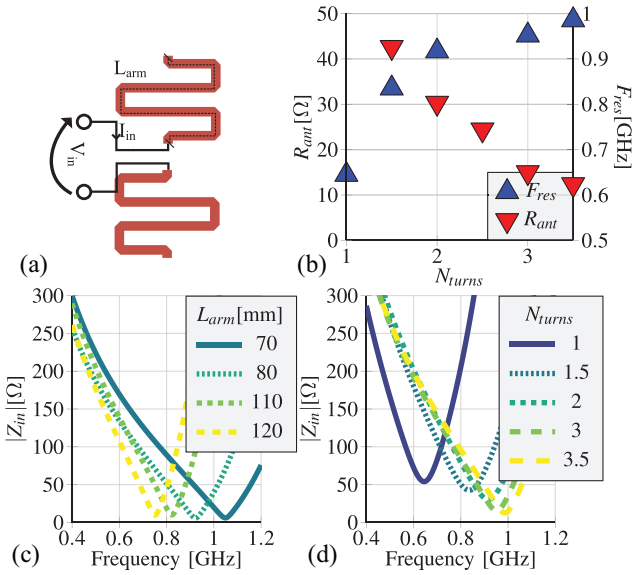

Fig. 2. Simulated response of a meandered RF antenna. (a) Drawing of meander antenna geometry, highlighting its excitation port and the arm length L_{ant}. In (a), for a fixed arm length L_{ant}, as the number of turns N_{turns} increases, overall antenna width increases and antenna length decreases. (b) Obtained R_{ant} (in red) and F_{res} (in blue) versus N_{turns}, showing that R_{ant} decreases monotonically with N_{turns}. (c) and (d) Magnitude of input impedance frequency response for various L_{arm}(c) and N_{turns}(d), for a reference width of 5 and a 2 mm gap.

A. Antenna Design

ADS Momentum®engine is used to evaluate the WuRx antenna's input impedance and radiation parameters. A reference substrate composed of a 16-mm thick FR4 layer with $\epsilon_r = 4.3$ sandwiched between two 17-μm thick Cu layers representing top (red colored) and bottom (blue colored) PCB metal layers, is used in Figs. 2 and 3.

A meander antenna [33] [shown in Fig. 2(a)] is often proposed for its ease of realization on PCB. When compared to a conventional dipole antenna, a meander antenna makes inherently more efficient use of the top metal layer, resulting in smaller form-factors. Simulation results in Fig. 2(c) show that the antenna resonance F_{res} scales inversely with respect to the arm length L_{arm} as expected for a dipole-like antenna.

The radiation resistance R_{ant} is mostly independent of L_{arm} at the resonance frequency, and instead, it decreases monotonically with N_{turns} as highlighted in Fig. 2(b). The minimum radiation resistance, $R_{\text{ant}} \approx 10\,\Omega$ realized in Fig. 2(c) is obtained for $N_{\text{turns}} = 3$, sufficient for this work. For more formal discussion, an investigation of the antenna response as a function of the number of meanders N_{turns} is discussed in [33].

A single-ended version of the meander antenna, shown in Fig. 3(a), is ultimately chosen for this application, leveraging the bottom metal ground pour as a path for return RF currents, resulting in an antenna excitation that can include a ground connection, breaking the symmetry of the differential dipole

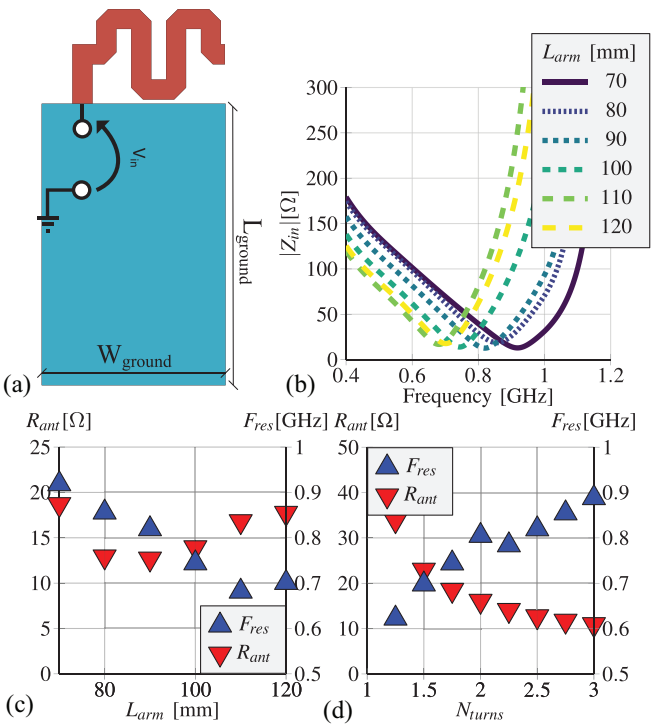

Fig. 3. Overview of the proposed WuRx monopole antenna, derived from the meander in Fig. 2. (a) Drawing of antenna geometry and antenna excitation port. (b) Magnitude of input impedance frequency response for various L_{arm}. (c) and (d) R_{ant} and F_{res} for combinations of L_{arm} and N_{turns}, showing analogue trends as in the meander antenna of Fig. 2.

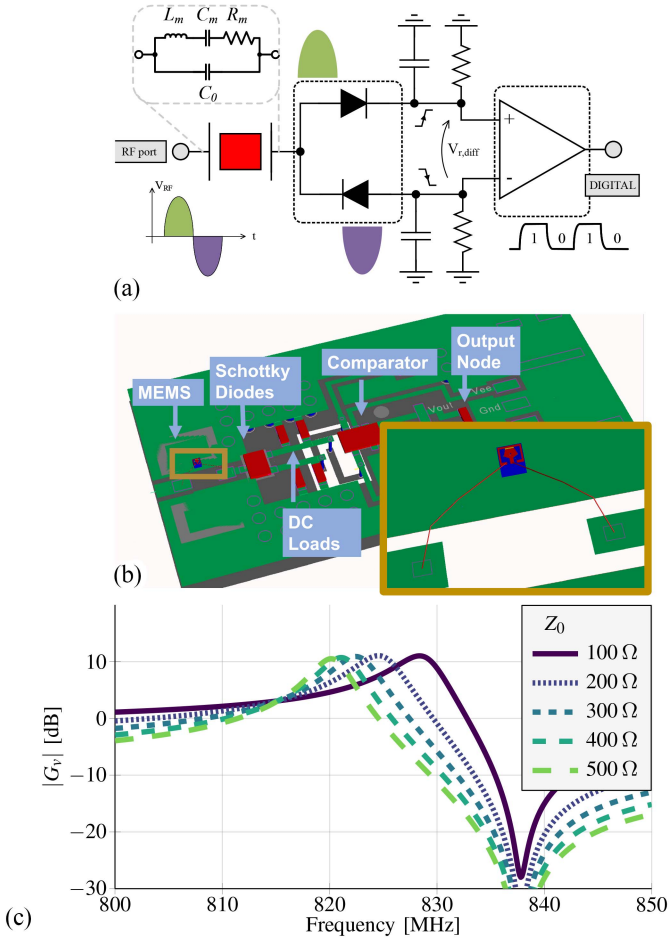

Fig. 4. (a) Circuit schematic of the proposed WuRx, composed of an MEMS resonator (modeled via its MBVD model) resonating a complementary actuated diode rectifier, followed by a commercial comparator used to discriminate bit stream. (b) EM simulation setup for RF voltage gain G_v of MEMS matched WuRx integrated on PCB, with the modeling of integration parasitics via wire bonding as shown in the inset. (c) Simulated G_v for various resonator impedances Z_0, obtained in Momentum engine, with SPICE-level modeling of an SBX201C Onsemi®Schottky diode used as RF rectifier. For the resonator, $k_t^2 = 7\,\%$, $Q_m = 550$ was assumed, to reflect the performance of the in-house fabricated FBAR resonator in Fig. 6. Z_0 represents the impedance of the static MEMS resonator capacitance C_0 at resonance.

and compatible with the single-ended grounded meander antenna.

The single-ended grounded meander antenna, shows similar trends as the differential one, as evident in Fig. 3. In particular, N_{turns} has a similar impact on R_{ant} [shown in Fig. 2(b) and (d)] providing an easy way to obtain low R_{ant}. Similarly, F_{res} is mainly dependent on both L_{arm} and only weakly dependent on N_{turns} as shown in Fig. 3(c) and (d).

While efficiency η_{ant} in the differential meander results in about 80 % due to the ohmic path required to implement a $\lambda/4$ stub, for the single-ended meandered design, an η_{ant} above 85 % is obtained in simulations, since only one arm contributes to the ohmic losses, i.e., due to being half of the differential counterpart.

B. Integration of MEMS Resonator on WuRx PCBs

A circuit deploying a complementary RF Schottky diode rectifier (SBX201C [34] from Onsemi) and a low-power comparator (TS391 [35] from Onsemi) are chosen to devise a simple WuRx asynchronous architecture [Fig. 4(a)], following the design proposed in [36], to down-convert and digitize the RF signal.

This prototype WuRx is implemented via commercially available components and it is intended to benchmark the benefits introduced by the custom RF passives designed in this work, and therefore, the obtained power consumption does not exhibit ultralow power custom IC designs, such as in [7], [22], and [23]. Rather, it is used as a proof-of-concept design of how passives can augment node sensitivity and selectivity in the presence of RF integration challenges.

One of the tuning knobs required to achieve a high Q_e is a high IC input reactance X_c. When operating at RF, every parasitic potentially impacts X_c by either introducing shunt capacitances to ground, or series stray inductance. To factor them in, the effect of wire bonding the MEMS resonator, the PCB traces, as well as packaging parasitics provided by manufacturer are included in an ADS Momentum®co-simulation platform [shown in Fig. 4(b) 'and (c)], capable of capturing EM effects induced by pads, traces, and wire bonds, as well as discrete components simulated from packaged parts.

An operational frequency of 817 MHz is set, falling within the RF range currently covered in some of the most popular IoT node applications, as discussed in Section I. A thin-film bulk-acoustic resonator (FBAR) operating in this frequency range is fabricated in-house and modeled in the EM setup as

shown in Fig. 4(b) (resonator in the inset). Details of FBAR fabrication are provided in [37].

Schematic and G_v simulation results obtained by using the FBAR resonator as a matching network and a back-to-back diode rectifier model are, respectively, shown in Fig. 4(a) and (c). The low junction capacitance, rated at $C_{j0} = 40\,\text{fF}$ in the datasheet, would result in a $X_c = 4.85\,\text{k}\Omega$. However, more than 100 and 85 fF are introduced by the packaging and SMD pads, respectively, resulting in a $X_c = 420\,\Omega$ at 817 MHz.

Considering that the simulation reflects conventional test setup for RF components, and, therefore, obtained by driving the matched stage with a 50-Ω source, an achievable $Q_e = 8.5$ is estimated from Fig. 1, and, therefore, an achievable gain G_v between 4 and 6, depending on k_p.

Therefore, the EM simulation results in Fig. 4(b) 'and (c) show that in absence of a tight integration process, the upper limit for X_c and, therefore, G_v is limited by packaging and/or wire bond parasitics, regardless of the resonator FoM, differently than for the ideal scenario discussed in Section II.

IV. Measurements

A. RF Components Characterization

Based on the design guidelines discussed in Section III-A, a PCB implementation of the proposed single-ended meandered antenna dipole is designed and characterized targeting WuRx communication bands, e.g., 800–900 MHz as in LoRa [38], and a low R_{ant}. The realized PCB antenna with results from an experimental campaign is in Fig. 5, obtaining good agreement between the EM model and the measured Z_{in}, both in R_{ant}, F_{res}, and radiation pattern.

A test setup is designed and implemented in the Kostas Research Institute [39] anechoic chamber in Burlington, MA, to investigate the radiation properties of the designed prototype. The DUT's antenna is positioned on an ETS-Lindgren automatic positioner and its yaw rotation axis is swept from 0° to 360°. A reference horn antenna with 10-dBi gain is oriented with its maximum gain direction interjecting the normal of the PCB plane, as shown in Fig. 5(c).

The experimental setup is run by exciting the horn antenna at the de-embedded resonance frequency 850 MHz so to identify the directivity on the XZ cut by rotating the antenna in the yaw axis, as noted in the picture, and recording at the same time the received power, properly scaled to take into account the low radiation resistance R_{ant}.

The antenna system is positioned at a distance of 13 m and using the Friis equation [40, Ch. 2] the realized antenna gain of the DUT is recorded as a function of the angle. A peak gain of 2 dBi, as shown in Fig. 5(d), closely resembles the predicted directivity of 2.5 dBi and efficiency of 83 %.

The frequency response at the antenna interface Fig. 5(b) is represented via Z_{in} rather than a more conventional S_{11} reflection. As the antenna is not matched to 50 Ω by design, the conventional S_{11} characterization does not capture meaningful information. In contrast, $|Z_{\text{in}}|$ highlights a series resonant peak at 850 MHz, showing a 11.5-Ω resonant input resistance. Given the complexity of directly measuring antenna efficiency [41], [42], antenna efficiency is estimated via the simulated

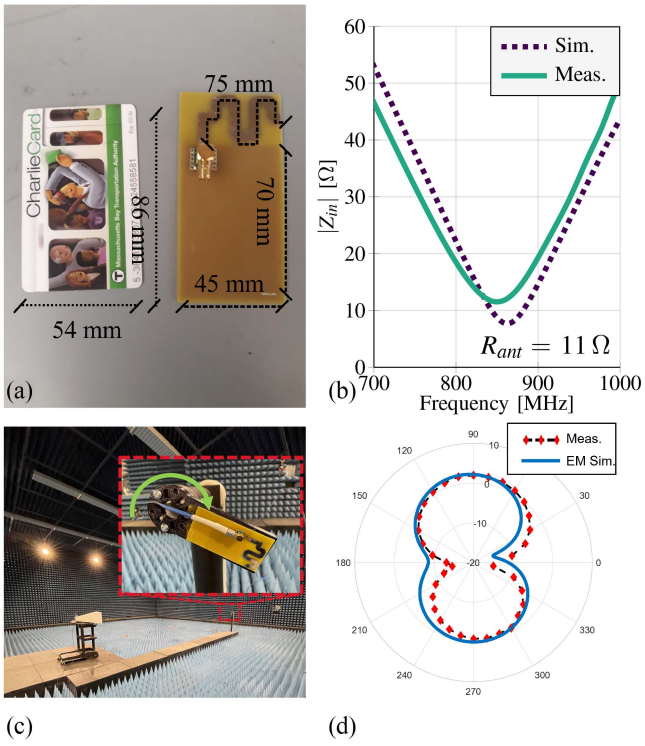

Fig. 5. Overview of LRA measurements. (a) Picture of the prototyped PCB Antenna with annotated critical dimensions, for an overall size of 33 cm^2, compared to the size of a credit card. (b) Antenna input impedance at the interface with the WuRx circuit, closely matching with the simulated response, with a resonance at 850 MHz, an input resistance at resonance 11.5 Ω, a radiation quality factor $Q_r = 10$, and a simulated efficiency of 83 %, leading to 2-Ω ohmic resistance and 9.5-Ω radiation resistance. (c) Radiation pattern test setup performed in the anechoic chamber. A reference horn antenna with 10-dBi gain is used in a two-port response characterization. The antenna under test is excited at resonance and an automatic angle sweep on the yaw axis is performed thanks to a motorized positioner. (d) Extrapolated antenna gain as a function of yaw angle, reaching a maximum of 2 dBi in excellent agreement with EM simulations.

Momentum results. Taking into account FR4 loss tangent and copper finite resistivity, an efficiency of 83 % is calculated, so that the overall input resistance can be broken down into a 2 and 9.5 Ω ohmic and radiation resistance, respectively.

A piezoelectric thin-FBAR [43], [44], [45], based on the vertical excitation of squeeze-film mode in a sputtered AlN film sandwiched between a Pt bottom electrode and an Al top electrode, has been fabricated in-house, and its fabrication process has been described in [46] and its cross section and SEM picture are represented in Fig. 6. This particular device showed $Q \approx 550$, coupling $k_t^2 = 7\,\%$, and a resonance frequency of 817 MHz [Fig. 6(c)].

B. Wake-Up Receiver Measurement

To better highlight the impact of RF termination on the measured G_v, two sets of experiments are presented: in the first scenario (Fig. 7) the WuRx is tested with an excitation coming from a 50-Ω coaxial cable. In the second one, in Fig. 8, the LRA and WuRx are integrated on the same PCB.

For the first setup, tested in a laboratory environment, an RF continuous wave () with variable frequency and power is fed to the front-end via coaxial cable, and the rectified dc

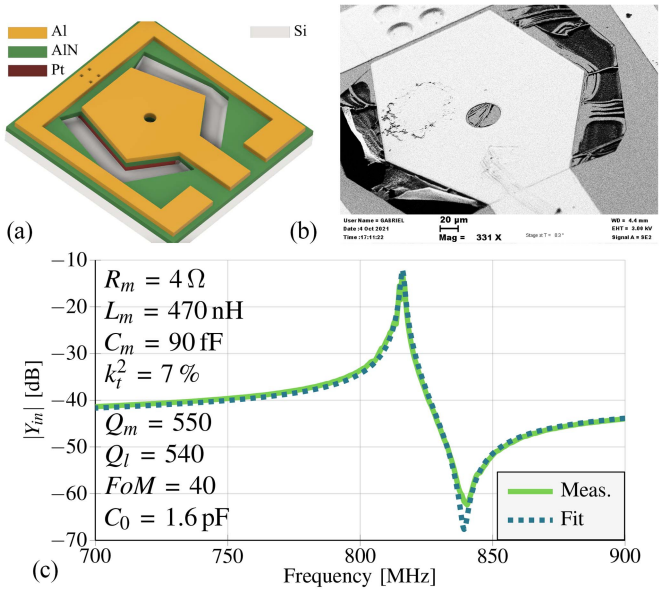

Fig. 6. Overview of MEMS resonator characterization. (a) 3-D model of the resonator cavity, composed of a stack of 80-μm Pt bottom metal layer, a 1 µm sputtered AlN film, and a 120-μm Al top metal layer. Details of fabrication in [37]. (b) Scanning Electrode Microscope picture of the fabricated device. (c) RF measurement of input impedance of the FBAR resonator, showing the fitted parameter according to the MBVD resonator model in Fig. 1(b).

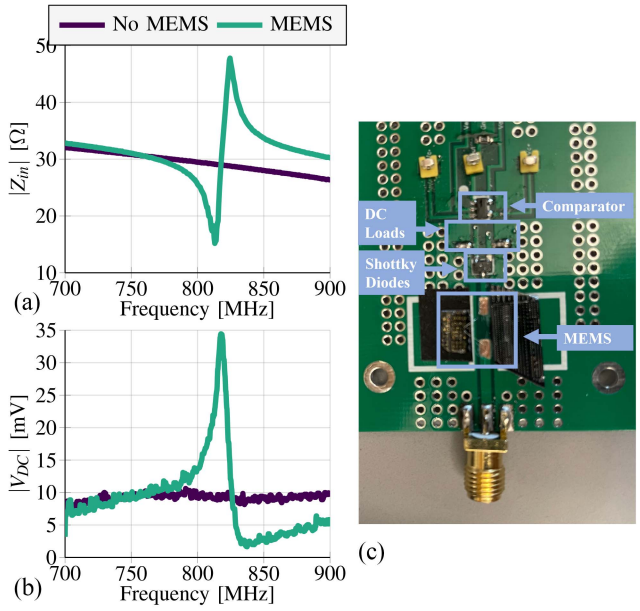

Fig. 7. RF Measurements of MEMS-matched WuRx terminated by 50-Ω source. (a) RF input impedance of the unmatched WuRx compared with the one matched with the in-house fabricated FBAR resonator, in the blue and green plot, respectively. The MEMS-matched WuRx PCB shows resonant-antiresonant response, with an input resistance at resonance approaching the R_m of the resonator (Fig. 6). (b) MEMS-matched WuRx shows a 12-dB higher dc rectification sensitivity for the same circuitry when excited with a −36-dBm continuous wave at resonance. (c) Picture of the designed PCB with discrete SMD components and the MEMS chip wire bonded to the circuit interface.

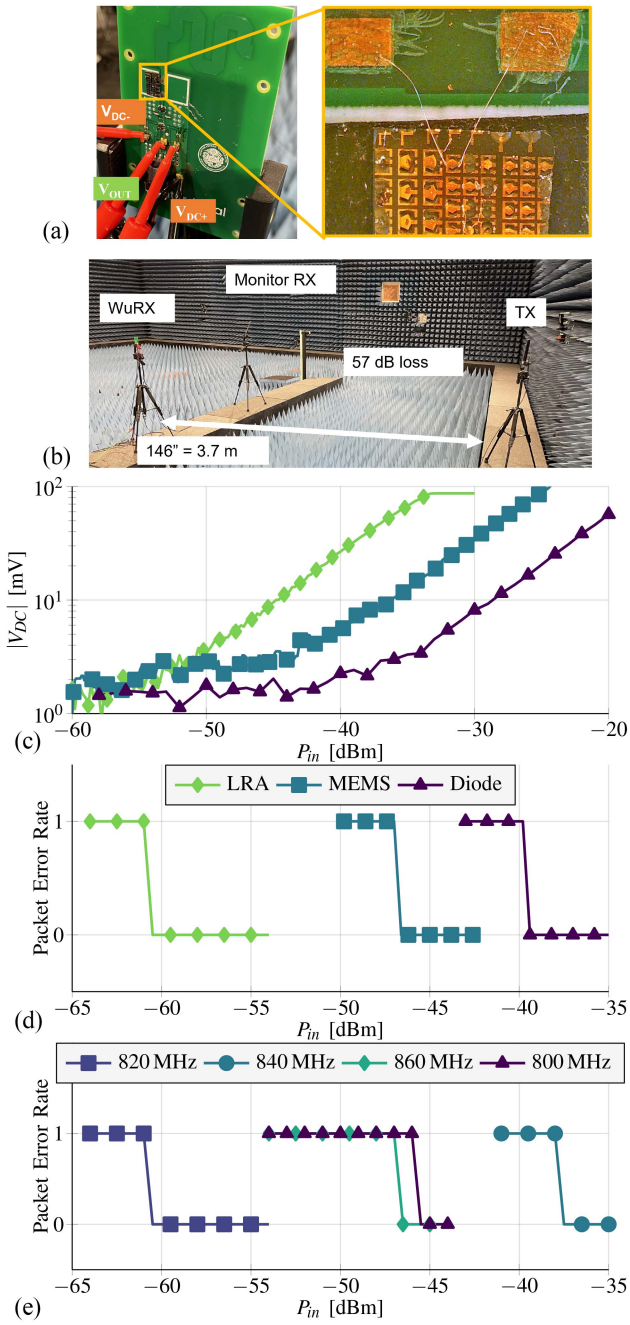

Fig. 8. (a) WuRx prototype composed of the custom LRA, connected to the WuRx board in Fig. 7 (in the inset, the hybridly integrated FBAR chip via gold wire bonds). (b) Communication link set up in anechoic chamber, with an ominidirectional TX antenna fed with the OOK signal, the WuRx placed 3.7-m away, and an auxiliary antenna to monitor Rx power. (c) DC rectified voltage at resonance for various RF power, respectively, for the unmatched WuRx, for the 50-Ω RF source WuRx of Fig. 7, and the one excited with the LRA, resulting in 11-dB extra sensitivity with respect to the 50-Ω counterpart. (d) PER for an OOK modulation at 817-MHz carrier with 1-kHz bitrate. The three boards achieved PER = 0 for thresholds of −40, −48, and −61 dBm, respectively. (e) PER sensitivity to blocker signals for the LRA WuRx. At ±20 MHz from 817 MHz 14 dB, and 23 dB rejection is measured.

voltage V_{DC} is measured at the comparator input, so to compare the rectification sensitivity between the MEMS-matched circuit and the unmatched one. The results are plotted in Fig. 7.

The center frequency of the system, $f_{res} = 817\,\text{MHz}$, is found close to the selected MEMS resonant frequency [Fig. 6(c)], confirming trends discussed in [47]. A board without MEMS is used as a reference, to highlight the relative gain measured on the board with MEMS. The measured gain

$G_v = 4$ (12 dB) is in partial agreement with the simulated performance. In this way, a moderate G_v is realized and the other proposed benefits of MEMS matching are experimentally validated. The sharp peak recorded in Fig. 7(b) is followed by an anti-resonance peak that ensures higher rejection in the near-band, in close agreement with the MBVD resonator model and the measured input impedance [Fig. 7(a)], resulting in a 23 -dB rejection between in-band and out-of-band response.

A second Rx experiment is designed to characterize the custom WuRx-Antenna PCB. The experiment is performed in the KRI [39] anechoic chamber in Burlington, MA, see Fig. 8(b), where the WuRx is placed at 3.7 m from Tx and a reference antenna is positioned at the same radial distance to monitor propagation loss of the Tx signal (57 dB).

In this setup, the overall center frequency shifts from the antenna resonance because of the high-Q MEMS resonator, resulting in an overall 817-MHz center frequency. Fig. 8(c) shows a direct comparison of the sensitivities when both systems are excited by a CW at resonance.

The rectified voltage is plotted against input power at resonance for a 50-Ω terminated WuRx and for the proposed LRA WuRx in Fig. 8(c) and compared with the unmatched rectifier as well, to emphasize the increased sensitivity at lower input powers. In this experiment, the limit of detection is set by the experimental setup, as no visible dc signal is measured below 50 dBm. The input thermal noise at the rectifier output is limited by the WuRX inherent filtering (estimated $60\mu V_{rms}$ in SPICE simulation), but a pair of unshielded, untwisted dc probes is used to connect the WuRx board to a DSOX400A Keysight oscilloscope, limiting the detection at around 1 mV with 64 averaged measurements, showing linear-in-db voltage rectification above −50-dBm input RF power.

A voltage gain of about 23 dB, 11 dB more than the gain obtained with a 50-Ω source, is measured for the LRA WuRx. The measured gain is compatible with a $Q_e \approx 20$ and $k_p \approx 2$. Note that Q_e is approximately five times larger than one realized on the 50-Ω source matched with the same resonator, which is consistent with an R_{ant} approximately five times smaller than 50 Ω. Fig. 8(d) ‘and (e) show measured results for the digital packet recovery experiment, verified using actual OOK modulated signals to send information over the air. A MATLAB interface is programmed so that a random sequence of 16 bits, independently generated at each experiment run, is used to modulate the RF carrier as an OOK sequence. The RF carrier is generated using a Tektronix TSG4104A signal generator, suitably amplified, and transmitted over the air in the controlled environment of the anechoic chamber. The WuRx comparator output is monitored by an oscilloscope, triggered by the first-bit edge in the Tx section.

An algorithm is used to record the voltage signal reconstructed by the WuRx and compare it with the input bit-stream to determine a packet error rate (PER) for different levels of input power. An input power threshold corresponding to the WuRx sensitivity is then determined.

Because of the relatively high power consumption of the commercial comparator (≈0.75 mW, approximately 0.5 mA at 1.5 V), no bits are lost above the threshold in both setups and, therefore, PER dropped quickly from 1 to 0 with no error, based on a statistic of 50 consecutive runs.

As shown in Fig. 8(d) ‘and (e), the LRA outperformed the 50-Ω source, confirming the 11-dB excess sensitivity measured in the dc rectification experiment, summing to a reported minimum detectable signal of −48 and −61 dBm, respectively, at 817 MHz. Note that in this test, the rectifier output is not monitored by the abovementioned dc probes, and at the same time the lower antenna input resistance contributes to a much lower noise floor at the comparator input—estimated to be, respectively, $25\mu V_{rms}$ in SPICE simulations.

TABLE I
RF PASSIVE VOLTAGE AMPLIFICATION IN SELECTED WURX DESIGNS

Ref.	Source	Thin-Film	Freq. [MHz]	*FoM*	G_v [dB]
[49]	Coax	LNB	404	327	22
[27]	Coax	LNB	88	157	14
[50]	Coax	AlN	59	32	20
[51]	Coax	AlN	2000	-	13
[37]	**Coax**	**AlN**	**817**	**38**	**12**
This Work	**Antenna**	**AlN**	**817**	**38**	**23**

Table I shows performance comparison with other examples in the literature of WuRx deploying MEMS resonators, showing that while this work outperforms WuRx based on AlN resonators thanks to the LRA, higher sensitivities can be achieved by using LNB resonators, opening to very interesting scenarios of high-gain WuRx when the antenna techniques discussed in this work are deployed in conjunction with such high FoM resonators.

Moreover, with the integration-aware modeling proposed in this work, the appropriated MEMS technology and RF integration platform can be selected so as to not limit the WuRx performance with parasitic effects when higher and higher RF carriers are considered.

V. CONCLUSION

A novel RF WuRx front-end for Narrow Band IoT is proposed in this work. The novel methodology leverages the co-design of PCB antennas with MEMS resonators to obtain high passive voltage amplification and sharp frequency selectivity, obtaining a scalable, inexpensive platform for next-generation IoT devices.

A PCB antenna design methodology is discussed and experimentally validated, and an in-house fabricated AlN FBAR micro-acoustic resonator is deployed to realize a WuRx with off-the-shelf diode rectifiers. The PCB platform is also used to show that passive voltage gain in a WuRx front-end is limited by parasitic effects rather than MEMS FoM in this frequency range with conventional antenna designs.

We experimentally validate the proposed WuRx, showing that the limits posed by integration parasitics can be lifted by using the proposed methodologies. A highest-in-its-class RF voltage gain of 23 dB is reported for an over-the-air prototype at 850 MHz, as the antenna and the MEMS are co-designed for high passive voltage amplification, at no cost in terms of power consumption, required antenna gain or improvements in the resonator FoM.

By leveraging the proposed approach, miniaturization, energy awareness, and large volume production of IoT node s can be made more and more attractive for next-generation cellular IoT devices and wearables at reduced link budgets.

ACKNOWLEDGMENT

The authors thank Matthew Kling and Adam Kolby from Northeastern KRI facility of Burlington, MA, USA, for their help with the measurement setup in the anechoic chamber. The authors also thank Michele Pirro and Piotr Kulik for fabricating the FBAR resonators used in this work.

REFERENCES

[1] I. F. Akyildiz, T. Melodia, and K. R. Chowdhury, "A survey on wireless multimedia sensor networks," *Comput. Netw.*, vol. 51, no. 4, pp. 921–960, 2007. [Online]. Available: https://www.sciencedirect.com/science/article/pii/S1389128606002751

[2] M. Kavre, A. Gadekar, and Y. Gadhade, "Internet of Things (IoT): A Survey," in *Proc. IEEE Pune Section Int. Conf. (PuneCon)*, 2019, pp. 1–6.

[3] N. R. Patel and S. Kumar, "Wireless sensor networks' challenges and future prospects," in *Proc. Int. Conf. Syst. Model. Adv. Res. Trends (SMART)*, 2018, pp. 60–65.

[4] D. Galante-Sempere, D. Ramos-Valido, S. L. Khemchandani, and J. del Pino, "Low-power RFED wake-up receiver design for low-cost wireless sensor network applications," *Sensors*, vol. 20, no. 22, p. 6406, 2020. [Online]. Available: https://www.mdpi.com/1424-8220/20/22/6406

[5] P.-H. P. Wang et al., "A near-zero-power wake-up receiver achieving −69-dBm sensitivity," *IEEE J. Solid-State Circuits*, vol. 53, no. 6, pp. 1640–1652, Jun. 2018.

[6] P. Bassirian, J. Moody, and S. M. Bowers, "Event-driven wakeup receivers: Applications and design challenges," in *Proc. IEEE 60th Int. Midwest Symp. Circuits Syst. (MWSCAS)*, 2017, pp. 1324–1327.

[7] A. Mittal et al., "A ±0.5 dB, 6 nW RSSI circuit with RF power-to-digital conversion technique for ultra-low power IoT radio applications," *IEEE Trans. Circuits Syst. I, Reg. Papers*, vol. 69, no. 9, pp. 3526–3539, Sep. 2022.

[8] "Motivation for new study item on ultra-low power wake up signal in rel-18, version 14.2.2," 3GPP, Sophia Antipolis, France, Rep. 36.331, 2021. [Online]. Available: https://portal.3gpp.org/ngppapp/TdocList.aspx?meetingId=60087

[9] T. Haque, H. Elkotby, P. Cabrol, R. Pragada, and D. Castor, "A supplemental zero-energy downlink air-interface enabling 40-year battery life in IoT devices," in *Proc. IEEE Global Commun. Conf.*, 2020, pp. 1–6.

[10] A. Taha, H. Elkotby, T. Haque, R. Pragada, and D. Castor, "Eliminating battery replacement throughout the useful life of IoT devices with limited-capacity batteries: Analysis and design of a zero energy air interface," in *Proc. IEEE Int. Conf. Commun. Workshops (ICC Workshops)*, 2021, pp. 1–6.

[11] *IEEE Standard for Information Technology—Telecommunications and Information Exchange Between Systems—Local and Metropolitan Area Networks—Specific Requirements—Part 11: Wireless LAN Medium Access Control (MAC) and Physical Layer (PHY) Specifications*, IEEE Standard 802.11ba, 2020. [Online]. Available: https://standards.IEEE.org/standard/802_11-2020.html

[12] D.-J. Deng, S.-Y. Lien, C.-C. Lin, M. Gan, and H.-C. Chen, "IEEE 802.11ba wake-up radio: Performance evaluation and practical designs," *IEEE Access*, vol. 8, pp. 141547–141557, 2020.

[13] G. Mahendra and T.-J. Lee, "How IEEE 802.11ba wake-up radio coexists with legacy WiFi?" *IEEE Commun. Lett.*, vol. 25, no. 10, pp. 3432–3436, Oct. 2021.

[14] R. Liu et al., "An 802.11ba-based wake-up radio receiver with Wi-Fi transceiver integration," *IEEE J. Solid-State Circuits*, vol. 55, no. 5, pp. 1151–1164, May 2020.

[15] "Internet of Things (IoT)." Dec. 2019. [Online]. Available: https://www.cablefree.net/wirelesstechnology/internet-of-things-iot/

[16] R. Aigner, J. Ella, H. J. Timme, L. Elbrecht, W. Nessler, and S. Marksteiner, "Advancement of MEMS into RF-filter applications," in *Int. Electron Devices Meeting Dig.*, 2002, pp. 897–900.

[17] S. Gong and G. Piazza, "An 880 MHz ladder filter formed by arrays of laterally vibrating thin film lithium niobate resonators," in *Proc. IEEE 27th Int. Conf.Micro Electro Mech. Syst. (MEMS)*, Jan. 2014, pp. 1241–1244.

[18] M. Rinaldi, C. Zuniga, C. Zuo, and G. Piazza, "Ultra-thin super high frequency two-port ALN contour-mode resonators and filters," in *Proc. Int. Solid-State Sens. Actuators Microsyst. Conf.*, 2009, pp. 577–580.

[19] *IEEE Standard Letter Designations for Radar-Frequency Bands*, IEEE Standard 521-2002, 2002. [Online]. Available: https://standards.ieee.org/ieee/521/768/

[20] L. Colombo, M. E. G. Klemash, T. M. Kiebala, S. S. Bedair, G. Piazza, and M. Rinaldi, "VHF and UHF lithium niobate MEMS resonators exceeding 30 dB of passive gain," *IEEE Electron Device Lett.*, vol. 42, no. 12, pp. 1853–1856, Dec. 2021.

[21] H. Bhugra and G. Piazza, *Piezoelectric MEMS Resonators* (Microsystems and Nanosystems). Cham, Switzerland: Springer Int., 2017. [Online]. Available: https://books.google.com/books?id=hYLgDQAAQBAJ

[22] H. L. Bishop, A. Dissanayake, S. M. Bowers, and B. H. Calhoun, "21.5 an integrated 2.4GHz −91.5dBm-sensitivity within-packet duty-cycled wake-up receiver achieving 2μW at 100ms latency," in *Proc. IEEE Int. Solid State Circuits Conf. (ISSCC)*, vol. 64, 2021, pp. 310–312.

[23] V. Mangal and P. R. Kinget, "A 0.42 nW 434 MHz −79.1 dBm wake-up receiver with a time-domain integrator," in *Proc. IEEE Int. Solid-State Circuits Conf. (ISSCC)*, 2019, pp. 438–440.

[24] L. Colombo, A. Kochhar, G. Vidal-Álvarez, Z. Schaffer, P. Simeoni, and G. Piazza, "Comparison between different MEMS laterally vibrating resonator technologies for passive voltage amplification in an RF front-end system," in *Proc. IEEE MTT-S Int. Microwave Workshop Series Adv. Mater. Processes RF THz Appl. (IMWS-AMP)*, Jul. 2018, pp. 1–3.

[25] L. Colombo, G. Michetti, M. Pirro, C. Cassella, G. Piazza, and M. Rinaldi, "Optimization of a series-parallel MEMS resonators configuration for passive voltage amplification in wake-up radios," in *Proc. Joint Conf. IEEE Int. Freq. Control Symp. Int. Symp. Appl. Ferroelectrics (IFCS-ISAF)*, 2020, pp. 1–4.

[26] P. Bassirian et al., "Nanowatt-level wakeup receiver front ends using MEMS resonators for impedance transformation," *IEEE Trans. Microw. Theory Techn.*, vol. 67, no. 4, pp. 1615–1627, Apr. 2019.

[27] B. Razavi, *RF Microelectronics* (Prentice Hall Communications Engineering and Emerging Technologies Series), 2nd ed. Upper Saddle River, NJ, USA: Prentice Hall Press, 2011.

[28] A. Mabrouki, M. Latrach, and Z. Sayegh, "Design and experiment of RF rectifiers for wireless power transmission," in *Proc. 13th Mediterr. Microw. Symp. (MMS)*, 2013, pp. 1–4.

[29] T. Wu, G. Chen, Z. Qian, W. Zhu, M. Rinaldi, and N. McGruer, "A microelectromechanical AlN resoswitch for RF receiver application," in *Proc. 19th Int. Conf. Solid-State Sens., Actuators Microsyst. (TRANSDUCERS)*, 2017, pp. 2123–2126.

[30] T. Ngo, A.-D. Huang, and Y.-X. Guo, "Analysis and design of a reconfigurable rectifier circuit for wireless power transfer," *IEEE Trans. Ind. Electron.*, vol. 66, no. 9, pp. 7089–7098, Sep. 2019.

[31] *IEEE Standard on Piezoelectricity*, ANSI/IEEE Standard 176-1987, 1988.

[32] L. Colombo, A. Kochhar, G. Vidal-Álvarez, and G. Piazza, "High-figure-of-merit X-cut lithium niobate MEMS resonators operating around 50 MHZ for large passive voltage amplification in radio frequency applications," *IEEE Trans. Ultrason., Ferroelect., Freq. Control*, vol. 67, no. 7, pp. 1392–1402, Jul. 2020.

[33] T. J. Warnagiris and T. J. Minardo, "Performance of a meandered line as an electrically small transmitting antenna," *IEEE Trans. Antennas Propag.*, vol. 46, no. 12, pp. 1797–1801, Dec. 1998.

[34] "SBX201C: Schottky barrier diode, 2V, 50mA, 0.25pF, dual CP." On Semiconductor. 2021. [Online]. Available: https://www.onsemi.com/products/discrete-power-modules/RF-diodes/sbx201c

[35] "TS391: Comparator, single, low power, 36 V." Onsemi. 2021. [Online]. Available: https://www.onsemi.com/products/signal-conditioning-control/amplifiers-comparators/comparators/ts391

[36] G. Michetti et al., "Hybridly integrated MEMS-IC RF front-end for IoT with embedded filtering and passive voltage amplification," in *Proc. IEEE Sens.*, 2021, pp. 1–4.

[37] P. Kulik, Y. Yu, G. Chen, and M. Rinaldi, "Highly linear magnetic-free isolator based on a time-modulated differential RF MEMS lattice filter," in *Proc. IEEE 32nd Int. Conf. Micro Electro Mech. Syst. (MEMS)*, 2019, pp. 871–874.

[38] "A technical overview of LoRa and LoRaWAN." LoRaAlliance. 2020. [Online]. Available: https://lora-alliance.org/wp-content/uploads/2020/11/what-is-lorawan.pdf

[39] "Anechoic chamber." KRI. Accessed: Jan. 13, 2023. [Online]. Available: https://facilities.northeastern.edu/anechoic-chamber/
[40] C. A. Balanis, *Antenna Theory: Analysis and Design*. Hoboken, NJ, USA: Wiley, 2015.
[41] P. Karstädt and A. Gupta, "Radiation efficiency measurement of communication antennas with wheeler cap method," in *Proc. Int. Students Young Sci. Workshop Photon. Microsyst.*, 2011, pp. 64–67.
[42] H. A. Wheeler, "The radiansphere around a small antenna," *Proc. IRE*, vol. 47, no. 8, pp. 1325–1331, 1959.
[43] Q. Chen, "Fabrication and characterization of aln thin film bulk acoustic wave resonator," Ph.D. dissertation, Dept. Mech. Eng., Univ. Pittsburgh, Pittsburgh, PA, USA, Sep. 2006. [Online]. Available: http://d-scholarship.pitt.edu/8460/
[44] R. C. Ruby, P. Bradley, Y. Oshmyansky, A. Chien, and J. D. Larson, "Thin film bulk wave acoustic resonators (FBAR) for wireless applications," in *Proc. IEEE Ultrasonics Symp. Int. Symp.*, vol. 1, 2001, pp. 813–821.
[45] R. Ruby, P. Bradley, J. Larson, Y. Oshmyansky, and D. Figueredo, "Ultra-miniature high-Q filters and duplexers using FBAR technology," in *Proc. IEEE Int. Solid-State Circuits Conf. Dig. Tech. Papers.*, 2001, pp. 120–121.
[46] M. Pirro et al., "Novel topology for a non-reciprocal MEMS filter," in *Proc. IEEE Int. Ultrasonics Symp. (IUS)*, Oct. 2018, pp. 1–3.
[47] L. Colombo, G. Michetti, M. Pirro, C. Cassella, G. Piazza, and M. Rinaldi, "Zero power X-cut Linbo3 MEMS-based radio frequency rectifier," in *Proc. Joint Conf. IEEE Int. Freq. Control Symp. Int. Symp. Appl. Ferroelectr. (IFCS-ISAF)*, 2020, pp. 1–4.
[48] M. Soliman et al., "An 18 nW −47 −40 dBm sensitivity 3-100 kbps MEMS-assisted CMOS wake-up receiver," *IEEE Trans. Circuits Syst. I, Reg. Papers*, vol. 66, no. 11, pp. 4439–4447, Nov. 2019.
[49] J. S. Fernandez et al., "Monolithic AlN MEMS-CMOS resonant transformer for wake-up receivers," in *Proc. IEEE Int. Ultrasonics Symp. (IUS)*, 2017, pp. 1–4.
[50] S. T. Block et al., "A 170 nW CMOS wake-up receiver with -60 dBm sensitivity using AlN high-Q piezoelectric resonators," in *Proc. IEEE Int. Symp. Circuits Syst. (ISCAS)*, 2017, pp. 1–4.

Giuseppe Michetti (Graduate Student Member, IEEE) received the B.S. and M.Sc. degrees from the Politecnico di Milano, Milan, Italy, in 2014 and 2018, respectively. He is currently pursuing the Ph.D. degree with the Electrical and Computer Engineering Department, Northeastern University, Boston, MA, USA.

He is currently working on nonlinear and time-variant RF circuits based on piezoelectric RF MEMS technologies for novel generation of RF front-ends. His research is based on MEMS applications for microwave circuits for mobile platforms.

Luca Colombo (Member, IEEE) received the B.Sc. and M.Sc. degrees in mechanical engineering from the Politecnico di Milano, Milan, Italy, in 2013 and 2015, respectively, and the Ph.D. degree in electrical and computer engineering from Carnegie Mellon University, Pittsburgh, PA, USA, in 2019.

He is currently a Postdoctoral Researcher with Northeastern University, Boston, MA, USA. His research focuses on RF MEMS for ultralow-power applications.

Gabriel Giribaldi (Student Member, IEEE) received the B.Sc. degree in physical engineering from the Politecnico di Torino, Turin, Italy, in 2018, and the joint M.Sc. degree in micro and nanotechnologies for integrated systems from the Politecnico di Torino, Turin, Italy, and Institut Nationale Polytechnique PHELMA, Grenoble, France, in 2020. He is currently pursuing the Ph.D. degree with Northeastern University, Boston, MA, USA, with research focus on piezoelectric MEMS resonators and ultrasound transducers, and RF electronics for ultralow-power applications.

Ankit Mittal (Graduate Student Member, IEEE) received the B.Tech. degree in electronics and communication engineering from Dayalbagh Educational Institute, Agra, India, in 2014. He is currently pursuing the Ph.D. degree with the Energy Circuits and Systems Group, Electrical Engineering, Northeastern University, Boston, MA, USA.

Prior to joining Ph.D. program, he worked as a Senior Design Engineer of NXP Semiconductors with a rich experience in SoC design and 5 memory testchip tapeout to his credit. His research interests include power management integrated circuit design, ultralow power biomedical circuits, and ultra low-power RF radio design.

Mr. Mittal was also the recipient of the Director's medal (Valedictorian Honor) from Dayalbagh Educational Institute.

Hussain Elkotby (Member, IEEE) received the B.Sc. degree (Hons.) from Suez Canal University, Ismailia, Egypt, in 2009, the M.Sc. degree in electrical engineering from Port Said University, Port Fuad, Egypt, in 2013, and the Ph.D. degree in electrical and computer engineering from Tufts University, Medford, MA, USA, in 2018.

He has joined the Technology Evolution and Prototyping Department, InterDigital Communications, Inc., Conshohocken, PA, USA, in April 2018, where he has been working as the part of the innovation team focused on the technology development of 5G and beyond generations of wireless networks. From September 2013 to December 2017, he was a Research/Teaching Assistant with the Department of Electrical and Computer Engineering, Tufts University. From 2010 to 2013, he concurrently held the position of a Teaching Assistant with the Department of Electrical Engineering, Port Said University, and a Research Assistant with the Department of Electronics and Electrical Communications Engineering, Cairo University, Giza, Egypt. His main research interests are in the areas of wireless communications, digital signal processing, information theory, and stochastic geometry.

Ravikumar Pragada (Member, IEEE) received the B.Eng. degree from Andhra University, Visakhapatnam, India, in 1995, and the M.S. degree in computer science and engineering from State University of New York at Buffalo, Buffalo, NY, USA, in 2000.

He is a Senior Director and the Senior Principal Engineer with InterDigital Communications, Inc., Conshohocken, PA, USA, where he is responsible for leading next-generation air-interface and system technologies. Since joining InterDigital Communications, Inc., in 2001, he led InterDigital's research and development teams covering incubation, prestandards Research and Development, standardization, technology and product development, and prototyping. Prior to joining InterDigital Communications, Inc., he was a Senior Engineer with the Wireless Research and Development Center, Motorola, Schaumburg, Schaumburg, IL, USA, where he was involved in developing wideband CDMA cellular communication systems. He is a prolific inventor with more than 200 granted or pending patent applications. His research interests include cellular, IEEE 802.11 (Wi-Fi®), and IoT technologies with current focus on ultralow-power communications, sub-THz systems, AI/ML applied to wireless, unmanned aerial systems/drones, millimeter wave, device-to-device communications, and beyond 5G architectures.

Mr. Pragada is a recipient of numerous innovation awards, including the InterDigital's Chairman's Award, the President's Award, multiple CTO awards as well as the Lucy Mahjobian Distinguished Publication Award. He served as the Vice-Chair for the IEEE 1920: Aerial Communications and Networking Standards Working Group and is currently InterDigital's lead delegate for Next G Alliance Technology WG and Green G WG.

Aatmesh Shrivastava (Senior Member, IEEE) received the Ph.D. degree from the University of Virginia, Charlottesville, VA, USA, in 2014.

Prior to the Ph.D. studies, he worked as a Senior Design Engineer with Texas Instruments, Bengaluru, India, from 2006 to 2010. From 2014 to 2016, he worked at the IoT start-up Everactive as a Senior Design Director, where he led the research and development of the energy harvesting and power management solutions. In August 2016, he joined Northeastern University, Boston, MA, USA, where he is currently working as an Assistant Professor with the Electrical Engineering Department. His research interests include self-powered and ultralow power circuits and systems, energy-harvesting and analog computing, hardware for AI, Internet of Things, and ultralow power bio-medical and neural circuits.

Dr. Shrivastava was a recipient of the 2022 CAREER Award from the National Science Foundation. He also serves as an Associate Editor for the IEEE OPEN JOURNAL OF CIRCUITS AND SYSTEMS.

Matteo Rinaldi (Senior Member, IEEE) received the Ph.D. degree in electrical and systems engineering from the University of Pennsylvania, Philadelphia, PA, USA, in December 2010.

He is an Associate Professor with the Electrical and Computer Engineering Department, Northeastern University, Boston, MA, USA, and the Director of Northeastern SMART a university research center that, by fostering partnership between university, industry, and government stakeholders, aims to conceive and pilot disruptive technological innovation in devices and systems capable of addressing fundamental technology gaps in several fields including the Internet of Things, 5G, quantum engineering, digital agriculture, robotics, and healthcare. He worked as a Postdoctoral Researcher with the University of Pennsylvania in 2011 and he joined the Electrical and Computer Engineering Department, Northeastern University as an Assistant Professor in January 2012. He is the Founder and the CEO of Zepsor Technologies, Boston, a start-up company that aims to bring to market zero standby power sensors for various Internet of things applications, including distributed wireless fire monitoring systems, battery-less infrared sensor tags for occupancy sensing and distributed wireless monitoring systems of plant health parameters for digital agriculture. He is also the Owner of Smart MicroTech Consulting LLC, Boston, a company that routinely provides consulting services to government agencies, large companies, and startups in the broad areas of micro and nano technologies, Internet of Things, wireless communication devices and systems, radio frequency devices, and systems and sensors. The research in his group is supported by several Federal grants (including DARPA, ARPA-E, NSF, and DHS), the Bill and Melinda Gates Foundation and the Keck Foundation with funding of $14+M since 2012. He has coauthored more than 140 publications in the aforementioned research areas and also holds ten patents and more than ten device patent applications in the field of MEMS/NEMS. His group has been actively working on experimental research topics and practical applications to ultralow-power MEMS/NEMS sensors (infrared, magnetic, chemical, and biological), plasmonic micro and nano electromechanical devices, medical micro systems and implantable micro devices for intrabody networks, reconfigurable radio frequency devices and systems, phase change material switches, 2-D material-enabled micro, and nano mechanical devices.

Dr. Rinaldi was the recipient of the IEEE Sensors Council Early Career Award in 2015, the NSF CAREER Award in 2014, and the DARPA Young Faculty Award Class of 2012. He received the Best Student Paper Award in 2009, 2011, 2015 (with his student), and 2017 (with his student) at IEEE International Frequency Control Symposiums, the Outstanding Paper Award at the 18th International Conference on Solid-State Sensors, Actuators and Microsystems, Transducers 2015 (with his student), and the Outstanding Paper Award at the 32nd IEEE International Conference on Micro Electro Mechanical Systems, MEMS 2019 (with his student).